Journal of Power Sources 196 (2011) 9058–9068

Contents lists available at ScienceDirect

Journal of Power Sources

journal homepage: www.elsevier.com/locate/jpowsour

Development of integrated fuel cell hybrid power source for electric forklift

T.M. Keränen[a,*], H. Karimäki[a], J. Viitakangas[a], J. Vallet[b], J. Ihonen[a], P. Hyötylä[b], H. Uusalo[a], T. Tingelöf[a]

[a] VTT Technical Research Centre of Finland, Espoo, Finland
[b] Department of Automation and Systems Technology, Aalto University, Espoo, Finland

ARTICLE INFO

Article history:
Received 31 October 2010
Received in revised form
16 December 2010
Accepted 7 January 2011
Available online 22 January 2011

Keywords:
Hybrid
Drivetrain
PEMFC
Forklift
Experimental
Modelling

ABSTRACT

A hybrid drivetrain comprising a 16 kW polymer electrolyte membrane fuel cell system, ultracapacitor modules and a lead-acid battery was constructed and experimentally tested in a real counterweight forklift application. A scaled-down version of the hybrid system was assembled and tested in a controlled laboratory environment using a controllable resistive load. The control loops were operating in an in-house developed embedded system. The software is designed for building generic control applications, and the source code has been released as open source and made available on the internet. The hybrid drivetrain supplied the required 50 kW peak power in a typical forklift work cycle consisting of both loaded and unloaded driving, and lifting of a 2.4 tonne load. Load variations seen by the fuel cell were a fraction of the total current drawn by the forklift, with the average fuel cell power being 55% of nominal rating. A simple fuel cell hybrid model was also developed to further study the effects of energy storage dimensioning. Simulation results indicate that while a battery alone significantly reduces the load variations of the fuel cell, an ultracapacitor reduces them even further. Furthermore, a relatively small ultracapacitor is enough to achieve most of the potential benefit.

1. Introduction

Proton exchange membrane fuel cells (PEMFC) are already applied in commercial civilian applications in which lead-acid batteries are the current technology (e.g. telecom, material handling vehicles) [1,2]. However, for other applications the lifetime of fuel cells remains an issue, especially in the case of cyclic operation and low humidity conditions. In addition, the cost of PEMFC systems continues to be high, which limits the number of applications where they can challenge the current dominant technologies.

Recent advances in electricity storage technologies help to tackle these obstacles. When a PEMFC power source is hybridized using batteries and/or ultracapacitors, the size of the PEMFC stack can be reduced and power transients become slower, since peak power is drawn from other energy storages. This enables both capital and volume savings. The less cyclic operation of the fuel cell also increases its lifetime and reduces system control challenges.

When fuel cells are hybridized, the task of defining the cost-efficient hybrid system solution becomes challenging. The size and configuration (i.e. topology) of the drivetrain components should be defined, and the total energy efficiency and the reliability should also be considered. The optimization of the system configuration for specific applications is highly dependent on the expected duty cycle and the cost of fuel and electricity.

The design and building of fuel cell and hybrid systems have recently been reported [3,4]. General existing issues and barriers have been recognized [5,6]. Evaluations of different drivetrain topologies have also been conducted and associated potential issues with power electronics in fuel cell system have been studied [7,8]. Energy flows between energy storages are controlled by power electronics in similar size hybrid systems [9–11].

Switched-mode converters add complexity, cost, electric losses and many practical problems, for example, control delays during fast transients. Consequently, passively coupled hybrid systems have potential benefits compared to actively coupled topologies. However, the definition of the size of the hybrid system components for materials handling applications has not been discussed in the literature. In addition, the description of the PEMFC systems used has typically not been done in sufficient detail.

In this paper, the design, building and characterization of two passive coupled triple-hybrid power sources are presented. The work consisted of two parts. In the first phase, a half-scale PEMFC hybrid system was built and tested in a controlled laboratory environment in order to study fuel cell hybrid dynamic behaviour and functionality. Effects on the ultracapacitor dimensioning in the triple-hybrid system were studied both in experimental tests with the laboratory hybrid system and by simulations. In the second phase, a full-scale power source with a similar hybrid system con-

* Corresponding author at: VTT Technical Research Centre of Finland, Fuel Cells, P.O. Box 1000, 02044 Espoo, Finland. Tel.: +358405658390; fax: +358 20 722 7048.
E-mail address: timo.keranen@vtt.fi (T.M. Keränen).

0378-7753/$ – see front matter © 2011 Elsevier B.V. All rights reserved.
doi:10.1016/j.jpowsour.2011.01.025

Nomenclature

PEMFC	polymer electrolyte membrane fuel cell
DC	direct current
PLC	programmable control logic
LEL	lower explosive limit
CPU	central processing unit
MMC/SD-Card	Multimediacard/Secure Digital-Card
CAN	controller area network
BoP	balance of plant
OS	operating system
RTOS	real-time operating system
TCP/IP	transmission control protocol/Internet Protocol
NutDAC	an open source control software library
PC	personal computer
CVM	cell voltage measurement
GUI	graphical user interface
CVM	cell voltage measurement
U	voltage
C	capacitance
R	resistance
SoC	state-of-charge
PI	proportional-integral (controller)
I	current
n	number of electrons transferred per ion
M	molar weight
F	Faraday constant
m	mass flow
ESR	equivalent series resistance
E/V	voltage

Units

V	volt
F	Farad
A	ampere
mbar	millibar
°C	degrees celsius
ppm	parts per million
kW	kilowatt
Ah	ampere hour
kWh	kilowatt hour
cm^2	square centimeter
MHz	megahertz
s	second
ms	millisecond
mV	millivolt
mΩ	milliohm
MJ	megajoule
lpm	litres per minute
As^{-1}	ampere per second

Greek letters

μC	microcontroller
λ	stoichiometry

Subscripts

BUS	common electrical rail
SC	ultracapacitor
MAX	maximum
BATT	battery
O_2	oxygen
CO_2	carbon dioxide
fc	fuel cell
cat	cathode

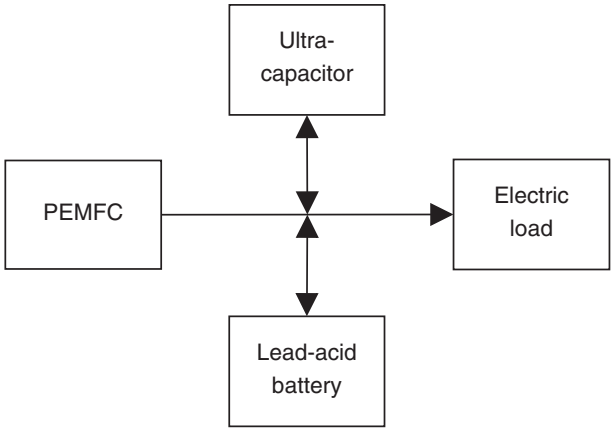

Fig. 1. Studied hybrid drivetrain topology.

figuration was constructed on a large counterweight forklift to be experimentally tested in real duty cycles.

2. Experimental

2.1. Hybrid drivetrain

The hybrid drivetrain was a triple hybrid system consisting of PEMFC stacks, ultracapacitor modules and lead-acid battery packs. The topology used is presented in Fig. 1. In the laboratory system, one of each of the three component units was connected in parallel to a DC bus with a nominal voltage of 40 V DC. In the forklift system, two units of each three components were connected in series to supply the 80 V DC required by the forklift.

The laboratory system was also tested without ultracapacitors, as a double hybrid combining a PEMFC and a battery, and by using a smaller 48 V 83 F ultracapacitor module in order to study the effects of the ultracapacitor and its dimensioning on forklift drivetrain performance.

The fuel cell system was protected using non-sparking automotive relays dimensioned for up to 500 A currents. Each of the relays was used to cut the main power lines and a 400 A Schottky diode was installed in the fuel cell supply line to protect the stacks from reverse current. Fuses were installed in each cable connecting the energy storages together to prevent dangerously high discharge currents, for example, in the case of short circuit.

An additional independent protection system was installed to protect the ultracapacitors from overvoltage and the battery from high currents on energy regeneration from the forklift load by a programmable logic controller. Voltage levels were measured, and the relays were used to switch the ultracapacitor connection and water-cooled resistor loads to the main bus, as required. The ultracapacitor was charged manually so that its voltage would be equal to that of the batteries before connecting for the first time. The voltage monitoring also prevented relay action if the voltage difference was more than 20 V.

The forklift power source was installed inside an empty battery compartment and a frame structure was built to house the components, with the exception of the 80 V DC lead-acid battery, which was located underneath the frame. Physical shock protection was installed in the frame to protect the sensitive components, and the system layout aimed to minimize issues related to coolant bleeding and reactant leaks.

2.2. Fuel cell system

The fuel cell system, as seen in Fig. 2, was operated at near-ambient pressure. The anode pressure was held constant at

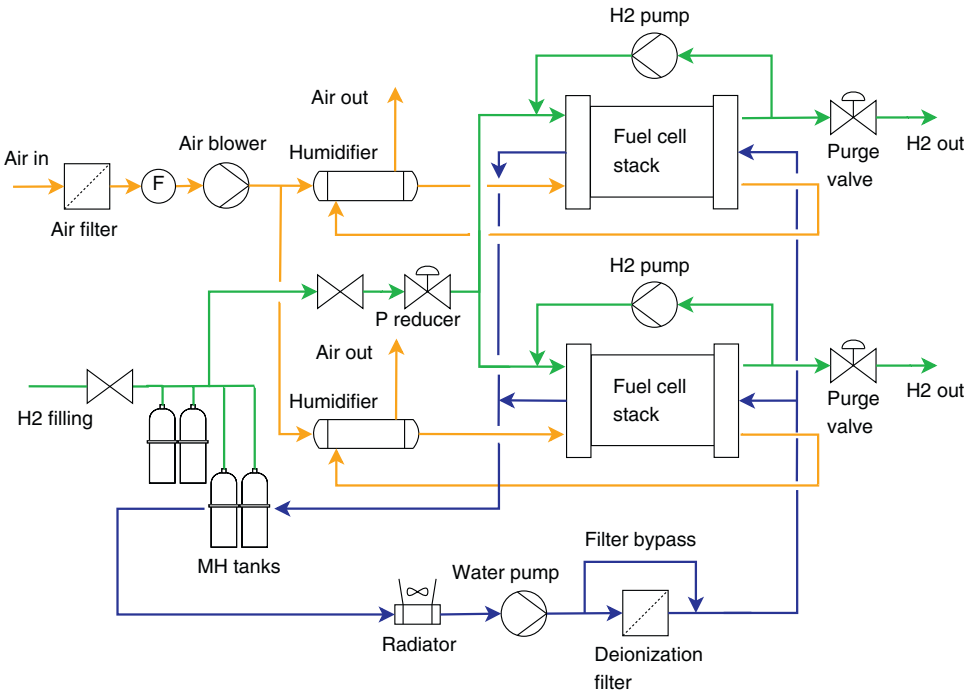

Fig. 2. Fuel cell system process diagram.

300 mbar (g) by a manual pressure regulator. A blower generated similar overpressure on the cathode at maximum flowrate.

The cathode supply was humidified with Permapure membrane humidity exchangers, while the anode gas was moistened by recirculating the moist outlet gas directly into the dry inlet gas using double-diaphragm pumps. A purge valve was installed on each PEMFC stack anode outlet to allow periodic ejection of excess moisture and inert gases.

De-ionized water was used as the coolant, and the circuit included a mixed bed ion-exchange filter to extend the coolant replacement frequency.

Hydrogen was stored onboard the forklift power source in metal hydride canisters for safety reasons. The canisters were connected in a common liquid cooling circuit with the PEMFC. Therefore, the metal hydride storage could offer additional cooling for the fuel-cell system while it was being discharged. The forklift hydrogen storage allowed up to 40 min of operation after each recharge.

A full list of the hybrid fuel cell system components is presented in Table 1.

The PEMFC shutdown procedure was triggered if the hydrogen concentration level within the system enclosure increased to over 50% LEL, hydrogen storage pressure dropped below 0.1 bar, or the

Table 1
Hybrid system components (laboratory and forklift systems).

	Laboratory experimental setup	Forklift power source
PEMFC stack	P8 (64 cells, 200 cm^2)	2 × P8 (128 cells, 200 cm^2)
Main auxiliary components		
Air blower	Domel 497.3.265–852	Ametek 117415E
Air filter	Donaldson FCX400045	Viledon FC F-0502
Air humidifier	Permapure FC300-1660-10HP	Permapure FC400-2550-7LP
H2 recirculation pump	Gardner Denver Thomas 118ZC	2 × Gardner Denver Thomas 118ZC
H2 pressure reducer	RHPS LRS(H)4	RHPS LRS(H)4
Power relay	Panasonic EP19024, Tyco Electronics EV200	Panasonic EP19024, Tyco Electronics EV200
Sensors		
Air mass flow meter	TSI 4235	Bosch HFM5-3.5
Water flow meter	OMEGA FPR-200	Aichi ND20-PATAAA
Temperature sensors	Tempatron, 10 kΩ NTC resistors (@ 25 °C)	Tempatron, 10 kΩ NTC resistors (@ 25 °C)
Pressure sensors	OMEGA PX2300	OMEGA PX2300
Current sensor	LEM DHR 300 C10, LEM HTR 200-SB	LEM DHR 300 C10, LEM HTR 200-SB
Main control system	Egnite software GmbH	Egnite software GmbH
	Ethernut 2.1/3	Ethernut 3
CVM unit	Vito CVM 96 channels	2 × Vito CVM 96 channels
Electric load	Amrel PLW12K-120-1200	Kalmar ECF-55
	12 kW	50 kW
Battery packs	Batteriunion AB 5EPzS300/5MDL60	2 × Batteriunion AB 5EPzS300/5MDL60
Capacity	300 Ah (12 kWh)	300 Ah (24 kWh)
Number of cells	20	40
Nominal voltage	40 V DC	80 V DC
Ultracapacitors	Maxwell Boostcap BMOD0083 and BMOD0165	2 × Maxwell Boostcap BMOD0165
Nominal capacitance	80 F and 165 F	80 F
Rated voltage	48.6 V DC	97.2 V DC
Surge voltage	50.4 V DC	100.8 V DC

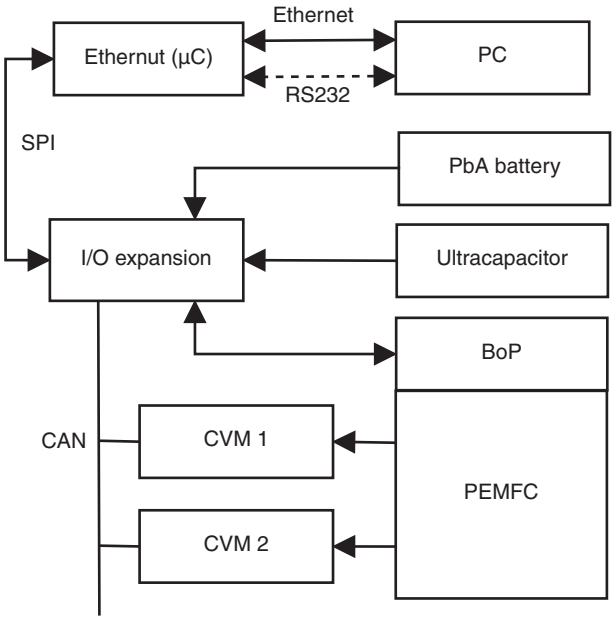

Fig. 3. Control system electrical layout diagram.

PEMFC outlet coolant temperature level moved outside the range of 0–60 °C.

The hydrogen for the laboratory system was supplied by an industrial quality pressure storage system, which allowed continuous operation of the fuel cell. Hydrogen used in laboratory experiments was a side product gas from an industrial electrolysis process with purity of 99.9%, CO2 content of <20 ppm and humidity of <20 ppm. In the case of the forklift power source, the hydrogen used was produced by an offsite steam reforming process. The purity of this hydrogen was stated as >99.9% by the supplier with THC content <5 ppm and humidity of <25 ppm.

2.3. Control system

The control system design is mostly based on open source hardware and software. The control system consists of a microcontroller unit and an I/O expansion board, a separate cell voltage monitoring unit and a laptop computer with graphical user interface and data logging features.

2.3.1. Hardware

The microcontroller board used was Ethernut 3 (by egnite GmbH). The microcontroller main board was equipped with an ARM7TDMI CPU running at 73.728 MHz, Ethernet controller and MMC/SD-Card socket. The microcontroller board provided computational capabilities, Ethernet connectivity, and local data storage. However, it did not have the necessary inputs and outputs to connect the actual hardware.

Separate instrumentation boards were designed for each power source. The instrumentation boards provided abundant I/O interface for sensors and actuators. The main difference between the two versions was the number of channels available. In addition, there was an extra CAN bus in the instrumentation board of the forklift for possible communications with a higher-level controller.

The cell voltages were measured by Cellsense cell voltage monitoring units, and the measurements were sent to the microcontroller via the CAN bus [12]. The control system hardware arrangement is described in Fig. 3.

2.3.2. Software

The software of the control system has been designed to control the fuel-cell power sources of different research projects. The source code has been released as open source under BSD license and is available online [13]. The source code is also suitable for generic real-time data acquisition and control applications for embedded systems. This is possible because the control software was implemented in a series of layers, when hardware abstraction is possible and reuse of code is easy. A simplified scheme of the software architecture is shown in Fig. 4. The top three layers (called I/O Drivers, NutDAC and User Application) were developed by Aalto University in cooperation with VTT, while the bottom layer (operating system and microcontroller, OS/µC) was supplied by egnite GmbH.

The OS/µC layer contains the operating system and the resources of the microcontroller. The NutOS operating system was used, which is the open source RTOS of the Ethernut project. The Ethernut project also provides a TCP/IP stack that is used for network communications.

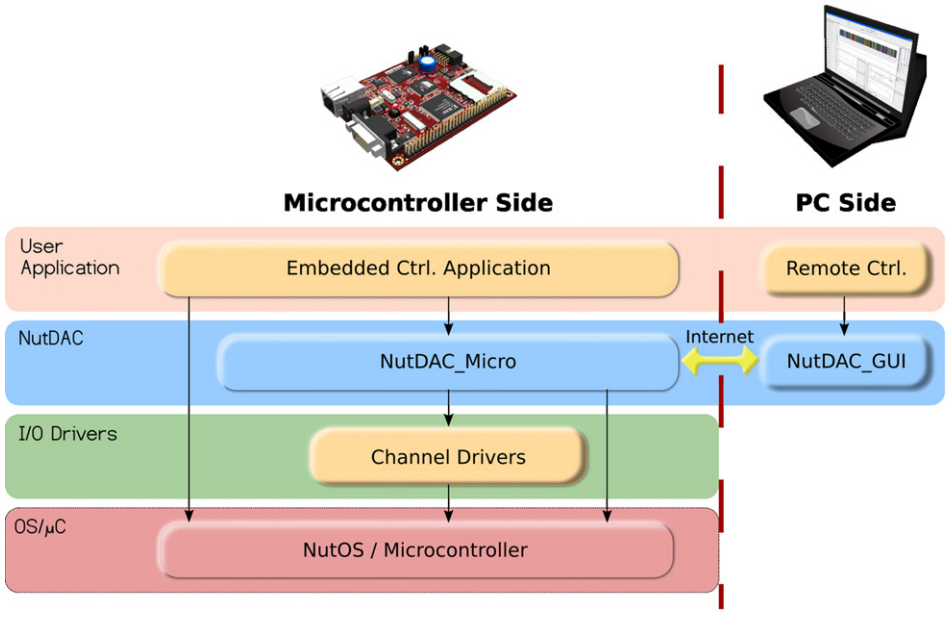

Fig. 4. Simplified scheme of the software architecture.

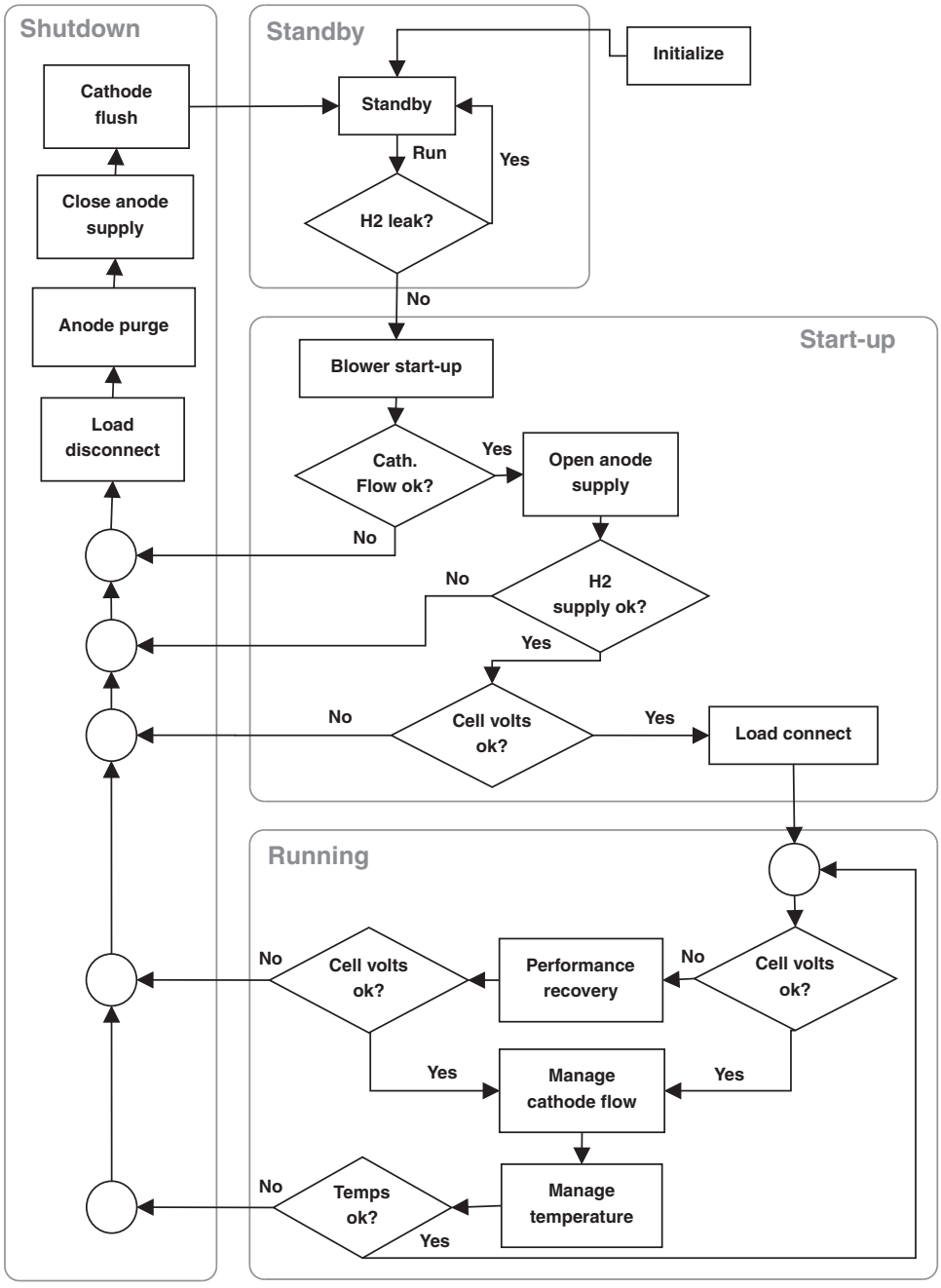

Fig. 5. Simplified control application state transition diagram.

The I/O Drivers layer contains all the routines that handle the communications with the external peripherals connected to the microcontroller in order to read sensors and command actuators. Each channel is typically associated with a hardware device (sensor or actuator).

The NutDAC (NutOS based Data Acquisition and Control) layer contains many useful tools that help to develop, use and maintain a typical real-time embedded control system. The libraries NutDAC_micro and NutDAC_GUI handle all the necessary coordination and synchronization mechanisms. NutDAC_GUI also provides tools for creating a fully featured GUI.

The application-specific fuel cell system control logic was implemented as a finite state machine in the top layer of NutDAC. It includes states for start-up and shutdown procedures, cell voltage management, load following cathode reactant flow control, system temperature management and proper transition conditions to move between them. The control system cycle rate was set to 200 ms for most of the measurements, with the exception of the cell voltages, which were updated every 500 ms by the cell voltage measurement (CVM) units. The user application also contains all of the fuel cell's safety related functions. Fig. 5 shows the execution order of the control application program in a simplified form.

2.4. Triple-hybrid simulation model

A simplified triple-hybrid model was developed consisting of PEMFC, lead-acid battery and ultracapacitor models. The hybrid model was coupled with a controllable load model, as seen in Fig. 6. All models were built in Matlab/Simulink and make use of the SimScape Electrical add-on library. More details about the model can be found elsewhere [14].

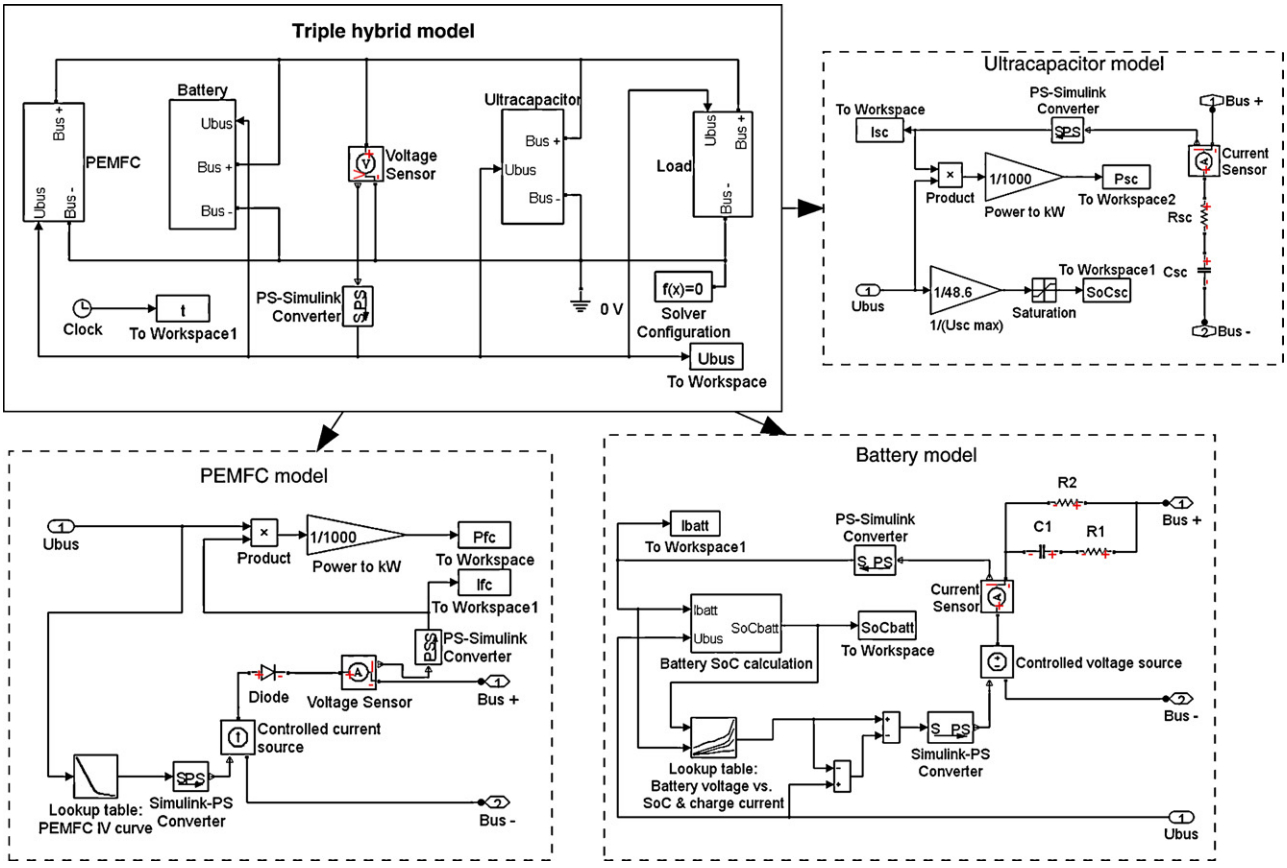

Fig. 6. Triple-hybrid Simulink model overview.

The fuel-cell model was based on an experimental polarization curve of the NedStack P8 PEMFC stack. A current–voltage lookup table was used to control a current source as a function of bus voltage, U_{BUS}. A diode was added in the circuit to prevent the current from flowing in the opposite direction, as in the real system.

The battery model was based on an equivalent circuit for lead-acid batteries [15]. It consisted of an ideal voltage source, a battery internal resistance R_2, and a capacitance C_1 with a resistance R_1 representing the dynamic properties of the battery.

The battery voltage was determined from a lookup table that was based both on experimental and manufacturer-supplied data. A "voltage compensation" was implemented by using two sum blocks that were used to cancel out the effect of the voltage over resistance and the capacitance blocks. The battery state of charge (SoC) calculation was done in a separate subsystem, based on a method described elsewhere [16].

Ultracapacitor equivalent circuit consisted of an ultracapacitor capacitance C_{SC} and series resistance R_{SC}. The SoC was calculated as a ratio between bus voltage U_{BUS} and ultracapacitor maximum operation voltage $U_{SC\,MAX}$. The parameters used for battery and ultracapacitor models are presented in Table 2.

Table 2
Lead-acid battery and ultracapacitor model parameters.

Lead-acid battery		Ultracapacitor	
		C (F)	R_{SC} (mΩ)
R_1	4 mΩ	165	1.75
R_2	33 mΩ	80	3.03
C_1	10 F	40	4.75
W_{BATT}	43.2 MJ	20	5.82

The load model was realized with a controlled current source feeding current against the energy storages. Drive cycles were read from current profile files.

2.5. Operating conditions and measurements

The PEMFC stack anode was operated with a mode combining dead-end operation and recirculation of anode gas. In this mode, the anode compartment is closed and hydrogen and water are purged when necessary. A constant anode gas recirculation rate was used during all measurements.

The hydrogen purge strategy was based on two trigger criteria that were executed in parallel; one based on a timer and the other on cell voltage levels. A timer-based trigger utilized a continuously updated purge frequency timer that depended on the load level of the fuel cell stack. Cell voltage monitoring consisted of two fixed voltage limits, referred to as "soft" and "hard" limit, and calculation of cell voltage deviation from the average. Crossing the soft limit of 500 mV, or exceeding the maximum allowed deviation of 50 mV, triggered the cell performance restoration procedure, consisting of an air flow pulse through the cathode and opening the anode purge valve for one control cycle (200 ms). The hard limit value of 300 mV triggered immediate disconnection of the load and the system shut-down procedure. A similar approach to cell voltage monitoring has been presented, for example, by Corbo et al. [17].

The cathode blower control strategy was realized with a combined feed-forward and heuristic control. The cathode blower has an internal, factory-tuned PI control loop with a linear relationship between analog control signal and motor rpm. The relationship between blower control signal and flowrate was extracted from experimental data obtained from dry cathode system tests. This was then utilized to define the cathode blower setpoint. The flow

resistance of the stack and the humidifier increased as water accumulated in the system. The effect of water accumulation on flow resistance was compensated by increasing the flowrate by a factor of approximately 1.15.

The blower flowrate followed a non-constant stoichiometry profile as a function of current drawn from the fuel cell stack. On low partial-loads, when higher step changes could be expected, the cathode stoichiometry was above 3 and gradually decreased with increasing load to around 2.5 at nominal stack current.

$$\lambda_{O_2} = -0.0068 \cdot I_{fc} + 4.2155 \quad (1)$$

$$m_{cat} = \frac{\lambda_{O_2} \cdot I_{fc} \cdot n \cdot M_a}{4F \cdot 0.21} \quad (2)$$

The sluggish blower response and the lack of load prediction in the control introduced a potential cathode reactant supply shortage during fast load transients. To mitigate this, an override of normal control signal calculation was done when a current step of 50 A or more was detected, and the blower was set to feed maximum flow for approximately 3 s.

Air humidity is not a directly controllable parameter in this type of system, as the air humidification is realized with the membrane humidity exchanger where the attained humidity depends on the flow rates and temperatures of the gases. The hydrogen humidification is done by mixing moist outlet gas with dry inlet gas using the hydrogen circulation pump. In principle, this could be used for humidification control. However, the used hydrogen pump was under-dimensioned and was only able to reach a recirculation ratio of approximately 0.5 at nominal fuel cell power. To obtain an optimum humidification rate, a proper recirculation rate in this system structure should be in the order of 100 lpm per stack. As a result, the hydrogen pumps were operated at maximum rpm regardless of the stack power, excluding the experiments in which they were deactivated.

The control of the cooling system was realized with the PEMFC coolant outflow's temperature rate of change. The operation temperature was kept mostly between 53 °C and 56 °C in the laboratory system and between 50 °C and 55 °C in the forklift power source. This is 10 °C lower than the maximum operation temperature specified by the stack manufacturer, but was chosen due to the low recirculation rate of the anode gas. A sample of fuel cell system operation parameters from the experimental tests is presented in Fig. 7.

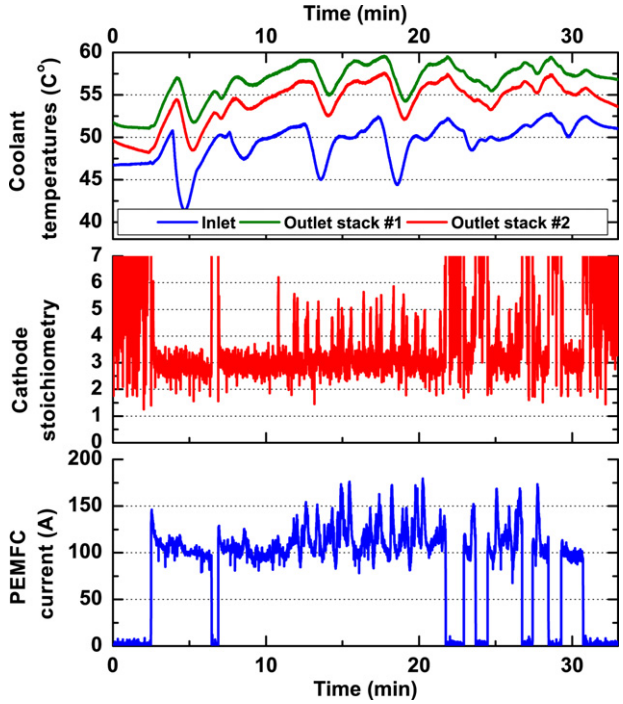

Fig. 7. Fuel cell system operation parameters during the forklift drive cycle.

2.5.1. Laboratory system

A simplified 60-s drive cycle was used in the measurements. The test cycle consisted of a constant base load of 35 A, and two consecutive high current peaks of 300 A for 2 s and 150 A for 2 s, respectively. The drive cycle was chosen to demonstrate the load sharing of different hybrid powertrain components during dynamic load current cycles.

The initial measurements were conducted with the double-hybrid system, which consisted of a PEMFC and a lead-acid battery connected in parallel. Two 90-min tests were performed, with initial battery SoCs of 0.5 and 0.8.

In the triple-hybrid system, an ultracapacitor module was added in parallel with the PEMFC and the lead-acid battery. Two hybrid tests of 2 h 45 min were conducted, starting from 0.3 battery SoC and with both ultracapacitor modules.

2.5.2. Forklift system

The system was initially characterized in the laboratory with an Amrel PLW12K-120-1200 programmable DC load. A Kalmar ECF-55 forklift was used for the outdoor system test drives. The ECF-55 has up to a 5.5 tonne lifting capacity and it is capable of utilizing regenerative braking energy. The test procedure included an indoor start-up and a brief warm-up without external heating, followed by outdoor driving tests with outdoor temperatures between −5 and −15 °C using a typical work cycle of a forklift.

During the warm-up, the PEMFC stacks were heated from the ambient to the operating temperature. This took approximately 10 min. During this procedure, the PEMFCs were charging the battery at an average rate of 100 A, corresponding to the charging rate of 0.33 C.

The drive cycle of the forklift consisted of four phases:

1. Driving the unloaded forklift for a distance of about 50 m.
2. Lifting a 2.4 tonne load while stationary.
3. Driving the loaded forklift, repeating the same route as in phase 1.
4. Lifting the load again, leaving it in place and restarting the cycle from phase 1.

Other experiments done on the 16 kW PEMFC system included short tests to compare the effect of disabling the hydrogen recir-

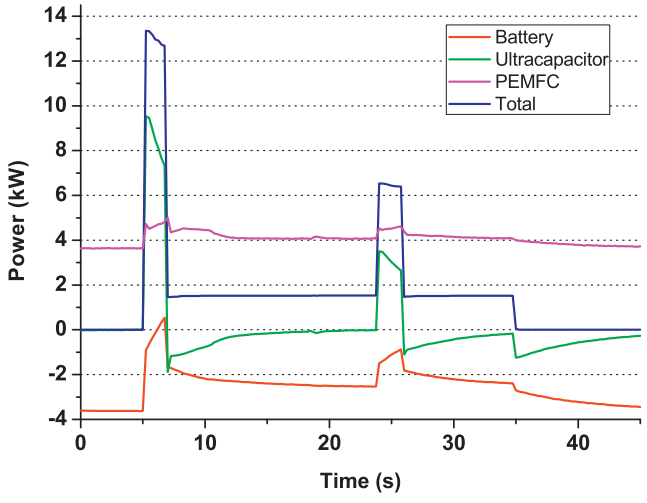

Fig. 8. Laboratory triple-hybrid system power distribution during the drive cycle.

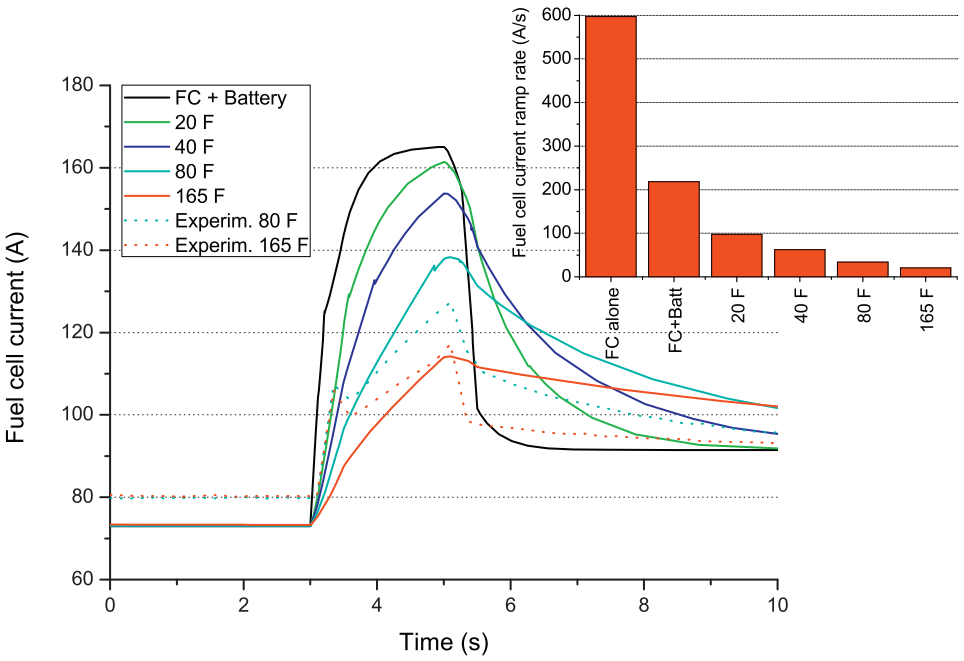

Fig. 9. Comparison of energy storage systems and PEMFC power distribution during a 300 A current peak on different ultracapacitor sizes (modelling and experimental results correlation).

culation pumps. Other energy storages were disconnected, and the fuel cell was operated on a constant load of 70 A using the programmable DC load.

3. Results and discussion

3.1. Laboratory system

The experimentally measured load power distribution between the hybrid system components is shown in Fig. 8. The results show that the ultracapacitor reached its maximum power of around 9.5 kW at the very beginning of the first power peak, supplying 70% of the total 13.5 kW peak power. Thereafter, the power of the ultracapacitor decreased, while the power of the PEMFC and the battery increased slowly. The battery was charged during almost the whole cycle due to the fairly low initial SoC of the battery pack, leading to a low bus voltage. When battery SoC increases, the PEMFC system delivers less power and eventually a steady-state SoC can be reached.

Simulated fuel cell power transients with different double- and triple-hybrid configurations are compared in Fig. 9. From the simulation results it can be seen that by hybridizing the fuel cell with only a battery, the power transient experienced by the PEMFC during the highest power peak could be decreased by 70%. However,

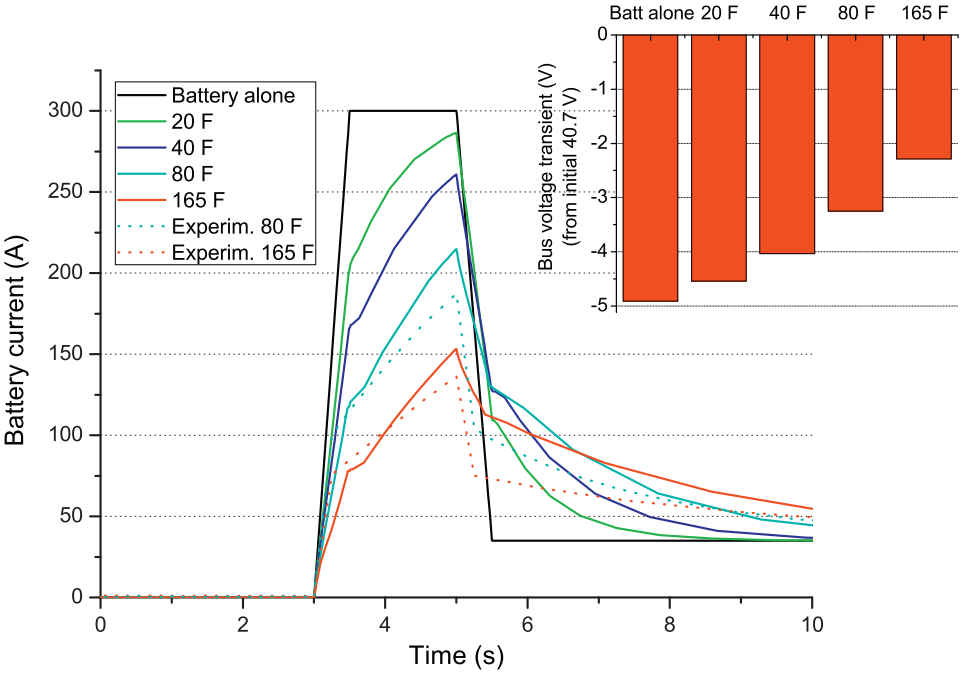

Fig. 10. Battery with ultracapacitor hybrid results. Battery SoC was about 0.5.

the current ramp rate is over 200 A s^{-1}, which is a formidable task for the control system.

The simulation results in Fig. 9 also show how in a triple-hybrid system a small ultracapacitor (20 F) is sufficient to reduce the current ramp rate by over 50%. However, to decrease the size of the power transient, a larger ultracapacitor capacity is needed, as shown in Fig. 9.

When the system was experimentally characterized with two commercially available ultracapacitor modules, the behaviour was very similar between the configurations, since both modules have very low equivalent series resistance (ESR) in comparison with the PEMFC and battery.

When simulation results are compared with experimental data, a clear deviation is observed. This is mainly due to the fuel cell model, which is a simple look-up table that does not take into account the different fuel cell operation conditions. The same is true for the battery model. However, by comparing the experimental measurements and simulations on the double-hybrid system, shown in Fig. 10, it could be stated that the battery model is not the main source of error.

The experimental data with 83 F and 165 F ultracapacitors correlates well with the modelled results. It should be noted that the duration of the current peak is very short and a different kind of load cycle may change the ultracapacitor capacity requirements.

The battery-ultracapacitor hybrid results shown in Fig. 10 illustrate how the battery current can be significantly reduced by coupling it with an ultracapacitor. The voltage drop behaviour is linearly dependent on ultracapacitor size.

3.2. Forklift system

Hybrid drivetrain load sharing during a part of the forklift duty-cycle is shown in Fig. 11. These results show how the fuel cell current varied between 80 A and 180 A during the load cycle, and the ultracapacitor supplied up to 80% of total power during the load peaks. Ultracapacitor voltage varied between 76 V and 95 V during the load cycle, with a corresponding SoC from 0.8 to 0.99, peak utilization of 19.7% of total capacity. The lead-acid battery SoC was around 0.3 at the start of each test session, from which it increased to around 0.45 towards the end of the experiment, with an average battery charging current of 50 A.

The nominal fuel cell load was approximately 9 kW_e (Fig. 12). It is also seen how the power of the fuel cell is determined by the bus voltage (76–95 V). When the system is in the start-up state, i.e. it is disconnected from the energy storage, the stack voltage is near the open circuit voltage. The points that are located outside the usual *I–E* curve are measured at this state of operation.

The cell voltages were stable and stayed within a 30 mV window during the maximum peak current of 180 A, as seen in Fig. 13, and the maximum rate of change encountered during actual driving.

The largest current ramp rates during the duty cycle were about 100 A s^{-1}. These are much smaller than the transient condition when the fuel cell was connected to the main bus, when a 113 A load step occurs. However, since this transient is predictable, it did not cause any major problem.

Auxiliary losses associated with balance of plant (BoP) components were measured during the test drives. The results in Fig. 14 show that a peak value of 16% for BoP losses is encountered during peak loads, while the cathode blower is controlled to its maximum power due to the fast load transient. Other major contributors to BoP losses include the cooling radiator fans which, while active, nearly double the system's electrical losses to 11% of the total current drawn from the stack. Since the test driving was done in cold conditions, the power demand of the radiator fans was very limited, and a low average value of 6.3% for BoP losses could be reached.

The effect of hydrogen recirculation was studied. The results shown in Figs. 15 and 16 demonstrate how cells 1 and 65, which

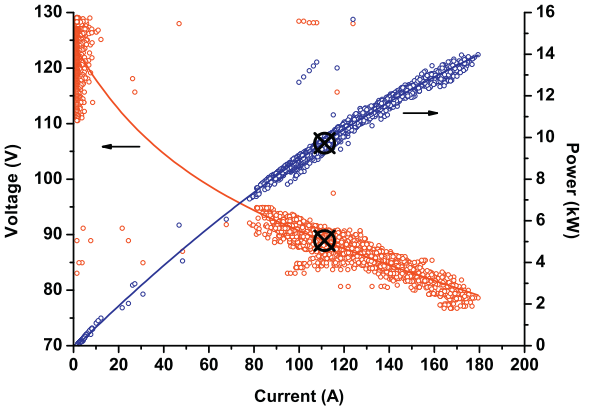

Fig. 12. PEMFC operating points during the forklift test drive cycle.

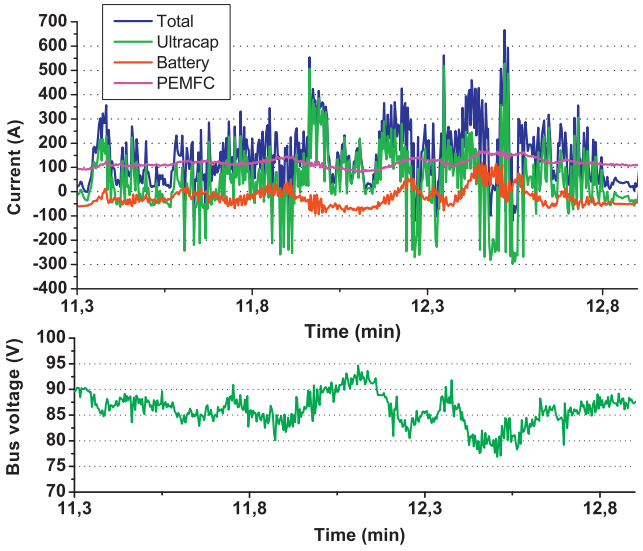

Fig. 11. Part of a forklift field test drive cycle.

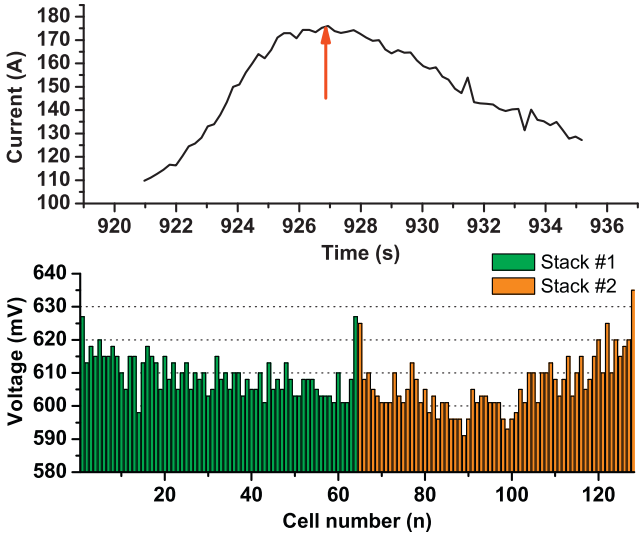

Fig. 13. Cell voltage deviation during load peak.

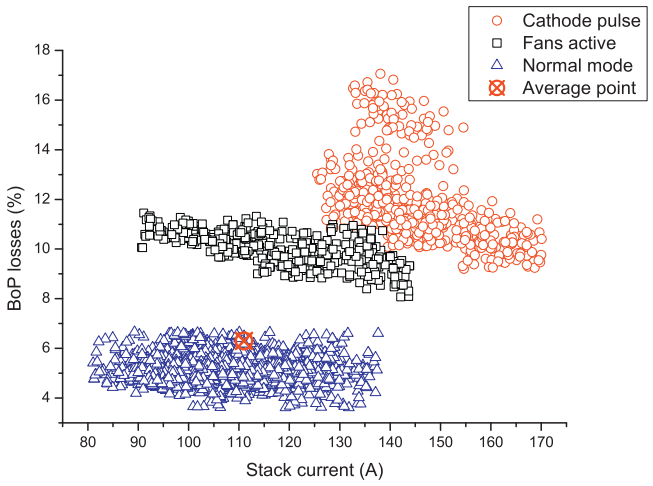

Fig. 14. BoP electric loss as a function of PEMFC current during the forklift drive cycle.

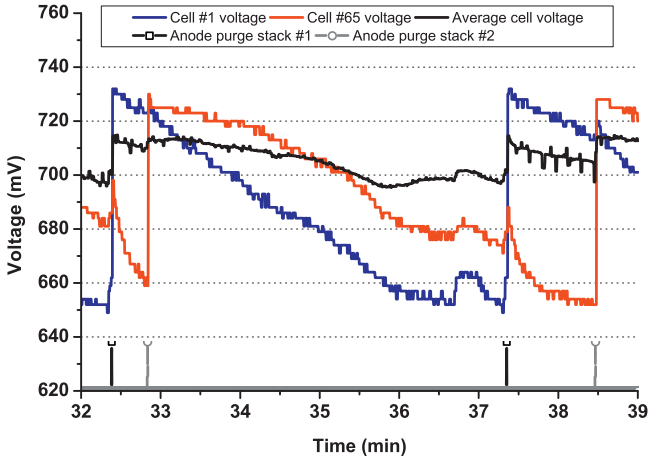

Fig. 15. Cell voltage variation while H_2 circulation was disabled.

are the closest to gas inlets and outlets in both stacks, have the lowest performance. During the dead-end operation, inert gases accumulate in the anode compartment. The pronounced effect of inert gases in cells 1 and 65 is possibly due to additional water accumulation in these cells, which amplifies the effect of inert gas accumulation.

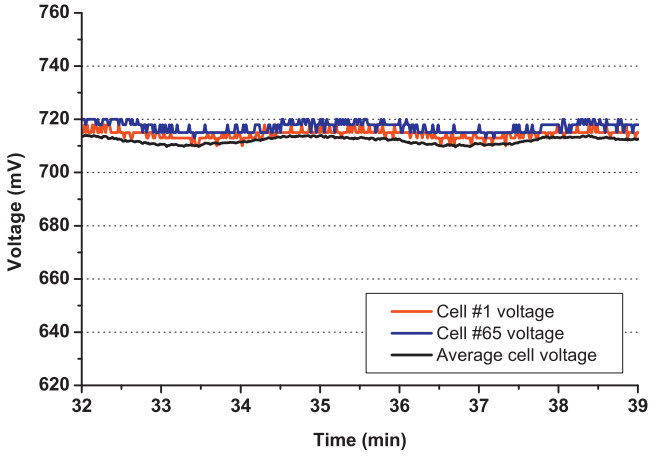

Fig. 16. Cell voltage variation while H_2 circulation was enabled.

Hydrogen recirculation is necessary for both the humidification of the membranes and distribution of inert gases. If recirculation is not needed for humidification purposes, a relatively small recirculation rate may be sufficient for the mitigation of the effect of the inert gases [18]. Since membranes are becoming more durable, it would be attractive to omit recirculation completely. However, the results in Figs. 15 and 16 show that omitting recirculation has a tremendous effect on cell voltage stability, which causes losses in fuel efficiency due to a need to increase the purge frequency.

4. Conclusions

Two triple-hybrid systems comprising a PEMFC power source, an ultracapacitor module and a lead-acid battery pack were successfully built and characterized. Characterization of the systems in the laboratory and in the test drives confirmed that triple-hybrid system components can be properly dimensioned using relatively simple simulation models. The characterization results indicate that passive configuration can be a real alternative to more complex configurations that utilize expensive power electronics. However, in passively coupled triple-hybrid systems, voltage variations are small and the system voltage should be close to the maximum voltage of the ultracapacitor module for the efficient use of ultracapacitor capacity. This, in turn, requires additional safety precautions to protect the ultracapacitor pack.

The laboratory characterization, field testing and simulations of triple-hybrid systems have verified the beneficial effect of passive coupling of ultracapacitors to the lead-acid battery and PEMFC. During the duty cycle, lead-acid batteries could manage moderate power transients, while ultracapacitors were needed for the larger load variations.

The system design and control system of the PEMFC power source were proven to be sufficient for hybrid system operation. The PEMFC power source could respond to very fast and large power transients. However, the need for the current ramp rate could be significantly reduced in double and especially in triple-hybrid systems. In triple-hybrid systems the size of the ultracapacitor does not need to be large to have a significant effect for the ramp rate of the PEMFC system. The decrease in the ramp rate relaxed the fuel control system response time requirements and helped to avoid issues related to air starvation.

The full evaluation of passive hybridization should be done by comparing the results with actively coupled configurations that utilize power electronics to control energy flows in the drivetrain. This requires both theoretical modelling and large amounts of experimental data from systems with both active and passive drivetrain topologies.

The hybrid topology research of this paper will be continued by investigation of actively coupled hybrid topologies. For PEMFC this is expected to help maintain low current ramp rates and a stable operating point, while on the other hand for ultracapacitors, a wider range of their available capacity can be utilized. In this work, a more advanced dynamic model is needed for the PEMFC system.

Acknowledgements

This work was conducted under the “Fuel Cell 2007–2013” technology programme of Tekes, Finnish Funding Agency for Technology and Innovation. The authors would like to thank the WorkingPEM project industry partners and the Ethernut community for their support. The authors are especially grateful to Cargotec, who provided the forklift and associated technical assistance during the project.

References

[1] A. Elgowainy, L. Gaines, M. Wang, Int. J. Hydrogen Energy 34 (2009) 3557–3570.
[2] P. Agnolucci, Int. J. Hydrogen Energy 32 (2007) 4306–4318.
[3] C. Bonnet, S. Didierjean, N. Guillet, S. Besse, T. Colinart, P. Carré, J. Power Sources 182 (2008) 441–448.
[4] P. Corbo, F. Migliardini, O. Veneri, J. Power Sources 181 (2008) 363–370.
[5] A. Pesaran, Advanced Capacitor Summit 2007, San Diego, CA, July 23–25, 2007.
[6] R.K. Ahluwalia, X. Wang, K. Tajiri, R. Kumar, DOE Hydrogen Program Review, Arlington, VA, May 18–22, 2009.
[7] S.M. Naylor, V. Pickert, D.J. Atkinson, 3rd IET Int. Conference on power Electronics, Machines and Drives, Ireland, April 4–6, 2006.
[8] R.S. Gemmen, J. Fluids Eng. 125 (2003) 576–585.
[9] M. Ouyang, L. Xu, J. Li, L. Lu, D. Gao, Q. Xie, J. Power Sources 163 (2006) 467–479.
[10] D. Gao, Z. Jin, Q. Lu, J. Power Sources 185 (2008) 311–317.
[11] P. Corbo, F. Migliardini, O. Veneri, Int. J. Hydrogen Energy 34 (2009) 4635–4644.
[12] VITO Cellsense CVM website, http://www.cellsense.eu/.
[13] NutDAC open source software package website, http://autsys.tkk.fi/nutdac/.
[14] H. Karimäki, Fuel Cell Hybridization for Vehicle Applications – Theoretical and Experimental Analysis, M.Sc. thesis, Tampere University of Technology, 2009, http://urn.fi/URN:NBN:fi:tty-201011231370.
[15] H.A. Catherino, J.F. Burgel, P.L. Shi, A. Rusek, X. Zou, J. Power Sources 126 (2006) 965–970.
[16] J. Bauman, M. Kazerani, IEEE Trans. Vehicular Technol. 57 (2008) 760–769.
[17] P. Corbo, F. Migliardini, O. Veneri, Renewable Energy 34 (2009) 1955–1961.
[18] R.K. Ahluwalia, X. Wang, J. Power Sources 171 (2007) 63–71.